Viscosity measurement from microscale convection at high pressure and temperature

Hannah B. Bartlett,[1] Natalia Gomez-Perez,[1,2,3] Michiel Hermes,[1,4] and R. Stewart McWilliams[1,*]

[1]*School of Physics and Astronomy and Centre for Science at Extreme Conditions, University of Edinburgh, EH9 3FD, Edinburgh, United Kingdom*

[2]*School of Mathematics, Statistics and Physics, Newcastle University, NE1 7RU, Newcastle upon Tyne, United Kingdom*

[3]*British Geological Survey, Edinburgh, Currie EH14 4BA, United Kingdom*

[4]*Soft Condensed Matter Group, Utrecht University, 3584 CC Utrecht, Netherlands*

(Received 2 November 2018; revised manuscript received 18 December 2019; accepted 24 February 2020; published 13 April 2020)

Measurements of induced thermal convection have been used to study fluid viscosity at simultaneous high pressure and temperature conditions. Direct observations of flow were made by tracking entrained particles in samples melted by laser heating during high-pressure confinement. Finite element models confirmed thermal convection as the origin of the detected motions, and were refined to assess the fluid viscosity. Observations of flow in ethanol partially melted in the laser-heated diamond anvil cell at 2–3 GPa point to a sharply rising viscosity at room temperature above the equilibrium solidification pressure, similar to that seen previously in methanol. The analysis shows that measurement of viscosity from convective flow in laser-heated fluids under static pressure is a promising strategy to determine viscosity at ultrahigh pressures, where high melting temperatures and small samples preclude application of traditional viscometric techniques. The data confirm theoretical predictions of detectable natural convection at ultralow Rayleigh numbers ($\mathrm{Ra} \ll 1$) in a microscopic system having sufficiently large temperature gradients.

DOI: 10.1103/PhysRevB.101.144202

I. INTRODUCTION

The flow behavior of fluids at high pressures is of broad importance, and the determination of fluid properties at relevant conditions, in particular the dynamic (or shear) viscosity, is essential. Accurately describing viscosity and flow at the high pressure and temperature conditions of deep planetary interiors is central for understanding the dynamics of planets [1,2]. Changes in fluid viscous (or viscoelastic) response with increasing pressure can closely correlate with modifications to other materials' properties, including liquid structure, melting points, and sound wave propagation behavior [2,3]. Viscous flows over small scales (of order micrometers) can play a role in the experimental determination of phase transformations at high pressures and temperatures, such as in measurements of melting under static compression [3–8] and the detection of insulator-metal transformation in fluid hydrogen under dynamic compression [9]. Thus, establishing high pressure viscosities experimentally can have broad impact.

However, measurements of viscosity are currently limited to lower pressures that are often insufficient to address outstanding questions. For example, knowledge of the viscosity of liquid iron alloy inside the Earth's outer core (>136 GPa) is critical for describing Earth's interior heat transport and magnetic field production, but this quantity is uncertain by several orders of magnitude [1] due to difficulties in reaching and extrapolating to relevant conditions [1,10]. To measure viscosity under pressure, experiments are typically conducted using a static high-pressure apparatus [1,11–14]. The highest pressure measurements of viscosity have been obtained to ∼11 GPa using diamond anvil cell (DAC) [12] and ∼16 GPa using multianvil cell [1] static compression techniques. These observe the gravitationally induced falling, floating, or rolling motions of particles (usually spheres) in the fluid, using resistive heating to melt samples [1,11,12,14]. At higher pressures, rising melting temperatures in most materials and smaller sample sizes combine to make the melting point harder to achieve by conventional resistive heating, while limiting the volume of fluid and thus the kinds of viscosity measurements that can be performed. No technique is yet available which could robustly measure viscosity at tens to hundreds of GPa. Strategies for higher pressure viscometry using shock wave experiments have led to unrealistically large estimates [14]. Theoretical predictions of viscosity have been employed at conditions that experiments can not reach directly, but still require benchmarking against high-pressure experiments [1,12].

The DAC high-pressure apparatus has been used to extend laboratory fluid studies to very high pressures and temperatures (beyond 100 GPa and 5000 K) using the technique of laser heating to melt the samples [4–8], though measurements sensitive to viscosity of fluids at these conditions have not been available. However, the existence of thermal convection of melts in these experiments, long inferred qualitatively from sample motions [4–7] could provide a window into the flow behavior of these extreme fluids and hence their viscosity, as recently established by numerical modeling [8]. Convective motion has been reported to very high pressure (e.g., to 200 GPa in Fe melts [5]), yet no approach to measure flow characteristics, such as velocity, has been developed.

*Corresponding author: rs.mcwilliams@ed.ac.uk

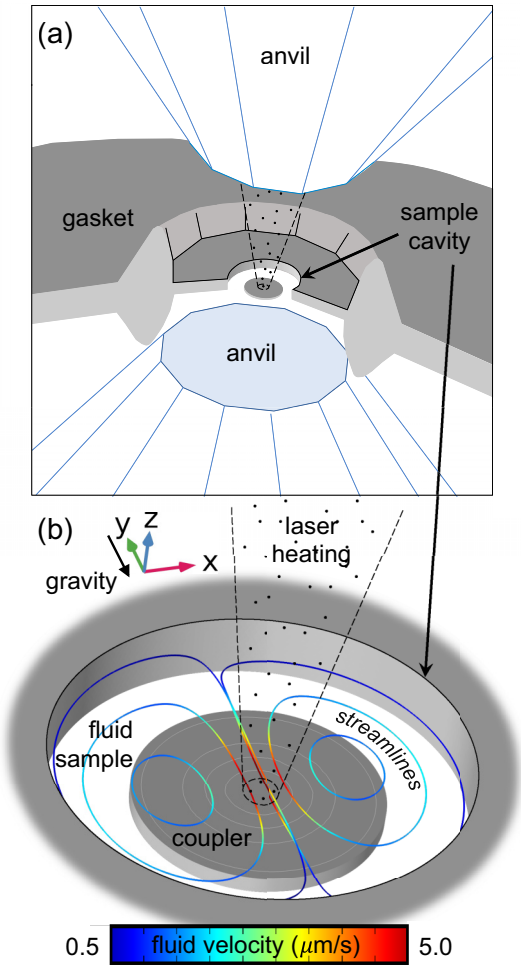

FIG. 1. Experimental configuration. (a) Configuration of laser-heated diamond anvil cell. Single-side heating was used. (b) Representative 3D finite-element convection model for a DAC sample. Streamlines are colored for local velocity. Grey concentric rings on the coupler surface indicate temperature contours of 350, 550, 750, and 950 K, from outside to inside. Thicknesses of the cavity, coupler, and sample (d) are 16, 4, and 12 μm, respectively; cavity and coupler radii are 50 and 30 μm, respectively; the fluid sample is presumed to have $\eta = 0.001$ Pa s, $\alpha = 2 \times 10^{-4}$ K^{-1}, and T_{melt} and $T_{\text{min}} = 300$ K (the coupler remains solid); sample (and coupler) ρ, specific heat C_P, and thermal conductivity κ are 1000 (9100) kg m^{-3}, 2000 (519) J kg^{-1} K^{-1}, and 10 (20) W m^{-1} K^{-1}.

Similarly, definitive proof that motions are thermal convective in nature, despite small length scales which normally suppress buoyancy-driven flow [6,8], remains to be obtained and is in itself a compelling proposition. Indeed, the convective Rayleigh number for the laser-heated DAC is many orders of magnitude lower than values typically associated with natural-convecting systems.

In this study, we perform direct detection of microscale convective flow under pressure in a laser heated DAC (Fig. 1). We study a sample of ethanol, for which the highest-pressure fluid viscosity measurements available, made nearly a century ago by Bridgman [13], are limited to 1.2 GPa.

II. METHODS

A confocal spectroscopy system for the laser-heated DAC [15] was adapted to provide video microscopy of the sample, with front and back illumination by white light, during heating by a continuous IR laser focused to a diameter of ~10 μm on the sample. The DAC axis and optical pathway were horizontal, i.e., perpendicular to the orientation of gravity. Sample dimensions were measured by microscopy and white-light interferometry. The cavity was of thickness 12−35 μm and diameter ~200 μm, contained between flat culets 300 μm in diameter. An iridium foil coupler, formed by the compression of iridium powder, was placed within the ethanol sample to absorb the IR laser, and remained solid during heating. Pressures were measured with ruby fluorescence [16] to be 1.9−2.7 GPa, at which conditions the ethanol sample was initially solid [17,18]. Chemical reaction at higher pressure (>2.8 GPa) and fluid phase separation at low pressure (<1.7 GPa) restricted the range of successful heating experiments on ethanol.

Localized melting of the ethanol, occurring on heating, was identified visually by the appearance of boundaries between the solid and the melt around the laser heated area, and confirmed by particle motions within the melt. Peak temperatures were estimated as 1000–1500 K based on emission spectroradiometry [15] at higher laser power, and finite element analysis of melt geometry (typical error was ~100 K).

Visualization of flow was provided by loose particles in the sample which moved with the flow; their trajectory and speed were measured after static background image removal from the raw video [19]. Videos were typically collected at a 30-Hz frame rate for 100-s intervals. Iridium particles left over from creating the coupler were most easily detected in practice, with ruby and other debris visually observed to exhibit similar motions but not readily trackable. Melting helped loosen particles from the surface of the diamonds or the coupler, but in some cases we also used an ultrasonic transducer mounted on the cell. The coupler pressing and particle seeding approach produced couplers with flat surfaces but irregular edges; these often floated slightly up into the ethanol medium during loading, and usually remained fixed in position during heating.

Finite-element modeling of the DAC sample, including the temperature profile of the system and the velocity of the flow inside liquid phases [8], was used to make initial predictions that were refined (cf., Ref. [20]) to assess sample transport properties. The finite element analysis used in this study adapts the two-dimensional spatial geometry for axially oriented gravity, previously described in Ref. [8], for gravity oriented orthogonal to the axis, requiring a model of three spatial dimensions.

In these models, liquid regions inside the sample chamber exhibit convection cells, where flow velocity depends on viscosity and liquid dimensions. The general behavior is shown in Fig. 1 for a simple, fully liquid sample with a circular chamber and coupler subjected to laser heating. The models reveal streamlines of motion that circle around the edge of the liquid region, and cross over the coupler near the laser focus, aligned with gravity. In the bulk of the liquid, velocity components oriented perpendicular to the axis (transverse

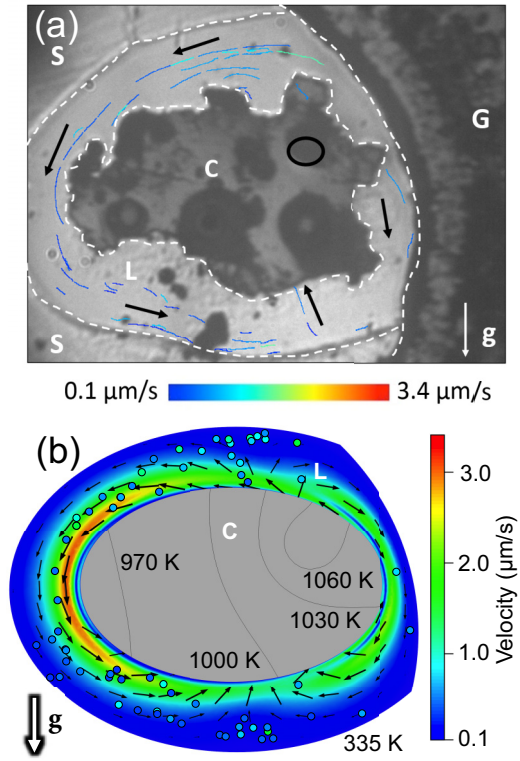

FIG. 2. Representative data set and finite element model for an experiment (sample SS40) on ethanol at 2.6 GPa. (a) Static background image (grayscale, 141 by 106 μm) with detected particle tracks (colored for maximum velocity); sample regions are G (W gasket), C (Ir coupler), S (solid sample), and L (liquid sample melted by laser heating); white arrow indicates the direction of gravity, black arrows the direction of flow. The black outline indicates where the laser was focused; here and at other points previously heated, a discoloration of the coupler was observed. (b) Finite element model of SS40 cavity showing the melted sample area, using simplified oval-shaped areas to represent the melt volume and coupler. The arrows and color map indicate the direction and speed of the local flow component perpendicular to the viewing axis, along the middle plane of the cavity. The black lines on the coupler surface are temperature contours. The measurements are black-outlined circles, positioned at track centers. Viscosity is given by Eq. (1), with E_{act} raised by 7% from the initial estimate (from 0.304 eV to 0.326 eV) to best fit the data while parameter B was kept constant at 6.9×10^{-6} Pa s. The model used sample (and coupler) ρ, C_P, κ, and α of 1200 (22500) kg m^{-3}, 2300 (133) J kg^{-1} K^{-1}, 0.171 (147) W m^{-1} K^{-1}, and 1.1×10^{-3} K^{-1}, respectively.

direction) are much larger than those oriented parallel to it (axial direction) for this orientation of gravity, according to our finite element modeling (Fig. 1). Thus, viewing motion along the axis [Fig. 2(a)] directly determines the convection velocities; this contrasts to the case of axial gravity [8] where substantial axial motion is anticipated.

Models were adapted to fit specific geometries of the experimental samples [e.g., Fig. 2(b)] to compare model velocities with experiment. The dimensions of the cavity, position and size of the coupler and molten region, the position and shape of the laser focus, and properties of the coupler and the sample were modeled [8]. In such detailed simulations, we set the geometry based on direct observations, and set the absorbed laser energy and peak temperature such that the observed position of the solid-melt boundary corresponds with the melt temperature.

Fluid viscosity η is initially estimated by fitting an Arrhenius model [1],

$$\eta = B \exp(E_{act}/k_B T), \tag{1}$$

to measurements up to 1.2 GPa near room temperature [13,21], where B is a constant, T is the temperature, and the activation energy is

$$E_{act} = E_{act0} + PV_{act}, \tag{2}$$

where P is the pressure, E_{act0} the activation energy at zero pressure, and V_{act} the activation volume. Fitted values are $B = 6.9(1.9) \times 10^{-6}$ Pa s, $E_{act0} = 0.139(7)$ eV, and $V_{act} = 0.0633(11)$ eV/GPa. This indicates values of 1–0.1 Pa s near melting under pressure. Within the studied pressure and temperature range (to 3 GPa and 1500 K), the extrapolated Arrhenius viscosity is within several tens of percent of extrapolations of other common models [11,22] of the data.

III. RESULTS AND DISCUSSION

Our experiments displayed the type of convective motion predicted by the numerical models. An example of the motion recorded is shown in Fig. 2(a) for a sample laser-heated at 2.6 GPa. The motions of the particles follow streamlines, moving around the outside of the coupler. As predicted, particles move over the coupler toward or away from the heating spot in a nearly vertical direction, antiparallel to gravity despite being denser than the fluid. The paths taken largely followed the contours of the coupler and melt boundary. Particles in close proximity to one another tended to move at the same speed and direction despite a size difference, thus it could be taken that the particles were well entrained in the flow and that the flow velocity was accurately determined. Convection speed across the experiments ranged from order 0.1 to 10 μm/s.

At these small length scales, convection flow speed U can be thought of as resulting from a balance of thermally induced buoyancy and viscous resistance forces [8,23], as in

$$U \sim \frac{\rho g \alpha \Delta T D^2}{\eta}, \tag{3}$$

where ρ is density, g the gravitational acceleration, α the volumetric thermal expansion coefficient, and ΔT the temperature difference across the thickness of the liquid region D. Assuming a constant fluid viscosity and adapting this scaling relation for the laser-heated DAC [8], we obtain

$$\eta = AC \frac{d^2}{v_{max}} \frac{(T_{max} - T_{melt})^3}{(T_{max} - T_{min})^2} \tag{4}$$

where v_{max} is the maximum sample flow velocity, d is the distance from the diamond surface to the coupler on the heated side, T_{max}, T_{melt}, and T_{min} are the maximum, melting, and minimum temperatures of the sample,

$$C = \rho g \alpha, \tag{5}$$

TABLE I. Maximum velocity in each experimental run which displayed convection. The viscosity was calculated using analytical scaling [Eq. (4)], with $A = 3.4 \times 10^{-2}$, $\rho = 1200\ \mathrm{kg/m^3}$ (Ref. [24]), $\alpha = 1.1 \times 10^{-3}\ \mathrm{K^{-1}}$, $T_{max} = 1100$ K, $T_{min} = 300$ K, and $T_{melt} = 335$ K (Ref. [18]).

DAC Sample	Pressure (GPa)	Maximum Velocity (μm/s)	d (μm)	Viscosity (Pa s)
SS40[a]	2.6	1.6	12.0	2.8×10^{-2}
SS2a	2.1	2.6	14.1	2.4×10^{-2}
SS4a	1.9	2.0	8.4	1.1×10^{-2}
SS2c[b]	2.7	2.4-7.0	8.6	$3.3-9.5 \times 10^{-3}$
SS4c[a]	2.4	8.7	25	2.2×10^{-2}
SS2e[a]	2.6	21.4-28.4	20	$4.3-5.8 \times 10^{-3}$

[a]Estimated d as a corrected average sample thickness due to incomplete thickness measurements.

[b]Some particles closer to the laser hot spot exhibited rapid, straight-line motion toward the hot spot with acceleration following a $1/r^2$ dependence (where r is the distance from the particle to the laser focus), unrelated to the direction of gravity; this was likely a non-convective phenomenon.

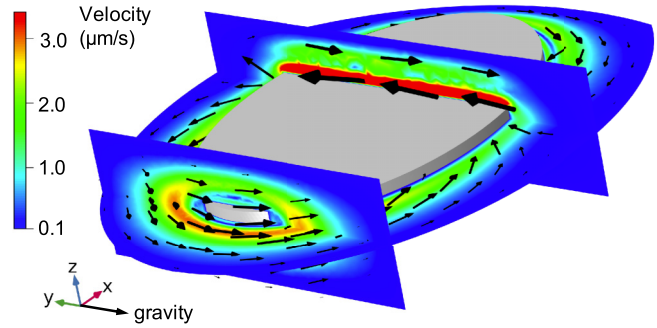

FIG. 3. View from the side of the finite element model of experiment SS40 (Fig. 2). The z direction is horizontal, pointing along the DAC axis, into the viewing and heating optics; the x and y directions are transverse, with x oriented horizontally and y vertically; gravity is directed in $-y$. Slices of local velocity are color maps; arrows show the sense of the flow nearby. The axial (z) component of velocity is included, but is negligible compared to the transverse components, as shown by the arrows. The transverse (x–y) slice of the velocity profile, sectioning through the coupler (grey), is as shown in Fig. 2. Two y–z slices show the variation in velocity with depth.

and A is a geometrical factor. Using the present 3D modeling, we observe $A = 3.4 \times 10^{-2}$ for a configuration where gravity is perpendicular to the axis, as used in these experiments, and $A = 1.3 \times 10^{-3}$ when gravity is parallel to the axis, in agreement with previous 2D modeling [8]. As A does not strongly depend on the specific configuration of the liquid region, in agreement with prior studies [8], it can be accurately considered a constant for a given orientation of gravity. The higher value of A (and thus, higher velocities) for gravity perpendicular to the symmetry axis results from the different direction of flow in the cavity, and the absence of fluid regions having a nearly plane-layer (Rayleigh-Bénard) geometry, which can suppress convection [8]. Consequently, the presently used radial orientation of gravity is a superior experimental configuration for observing convective motions, in that flow is detectable for viscosities an order of magnitude larger than for an axial orientation [8].

Viscosities calculated from the scaling law [Eq. (4)] for the experimental runs that displayed convective motion (Table I) range from 3 to 30×10^{-3} Pa s, with a best value of $17 \pm 9 \times 10^{-3}$ Pa s. These values are similar to the viscosity of fluid ethanol at high pressures and room temperature [13], though all present measurements are at pressures in excess of the room-temperature solidification point [17]. Indeed, the Arrhenius model [Eq. (1)] fitted to the low-pressure data predicts that these viscosities correspond to 420–570 K at ~2.6 GPa, confirming that the measurements detected flow in a hot lens of melt produced at the laser heated area. The viscosity thus determined is an average value for the melted region, corresponding roughly to a volumetric average over the temperatures in the melt, from the melting point (~340 K at 2.6 GPa [18]) to the maximum temperature set by the laser power (~1000–1500 K). In addition to limitations posed by the assumption of constant melt viscosity in a system with large temperature gradients, particle tracking did not necessarily sample the fastest flow speed [i.e., v_{max} in Eq. (4)]. Thus viscosities determined in this manner from Eq. (4) are approximate.

A detailed finite element analysis of the observed local flows, incorporating an accurate sample geometry and realistic temperature distribution, is needed to further refine the estimates of viscosity. This is made here via a detailed examination of a data set at 2.6 GPa [Fig. 2(a)], which has the greatest amount of detected particle tracks. The coupler, situated close to the gasket at the edge of the circular sample chamber, was modeled as approximately oval shaped as was the melt surrounding it. The model was initialized using the Arrhenius viscosity model fit to low-pressure data, which predicted velocities roughly 50% higher than observed on average for this data set. To better fit the observations, the activation energy at 2.6 GPa was adjusted upward by 7%, increasing viscosity at a given temperature and reducing flow speeds, producing the improved fit shown in Fig. 2(b). A constant viscosity model with $\eta = 3 \times 10^{-2}$ Pa s also adequately represented the data, consistent with the initial analytical estimate made for this experiment assuming constant viscosity (Table I).

In either model, while the range of predicted velocities and local flow trajectories agreed well with those observed, discrepancies in local magnitudes and relative speeds across the sample are noted; e.g., while we observe faster movement closer to the laser heating spot, the model predicts faster movement further away from it. These are attributed to differences between model and experimental geometries, such as the irregular outer boundary of the coupler in the experiment, which affects flow immediately adjacent to the boundary while flow away from the boundary remains the same; and to particles traveling at different depths within the sample (Fig. 3), which is accounted for in model fitting.

As the present data alone are not sufficient to establish the appropriate model formulation for viscosity, we consider the Arrhenius model, fitted to and validated by the low-pressure data, and tested against and adjusted to the present high pressure data, to provide the most accurate description of

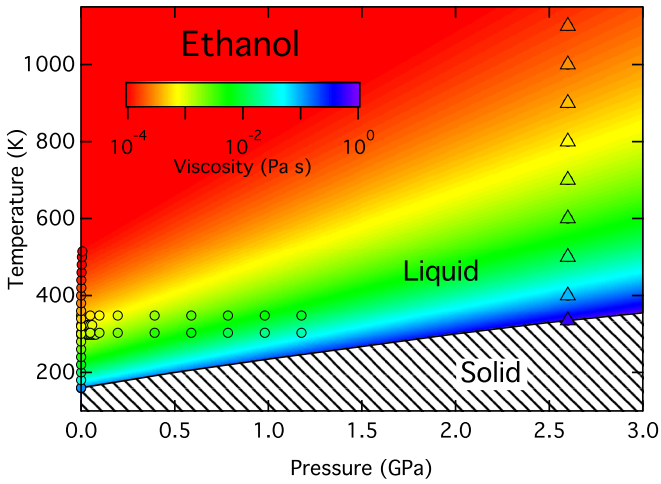

FIG. 4. Viscosity of fluid ethanol as a function of pressure and temperature. Present results are triangles, taken from the model refinement of convection data in the laser-heated DAC (Fig. 2) in the accessed temperature range. Previous data, at low pressure and temperature, are circles [13,21,25]. The color map is the Arrhenius model [Eq. (1)] fit to all the data. The melt curve is the black line [18], with the solid stability field shaded.

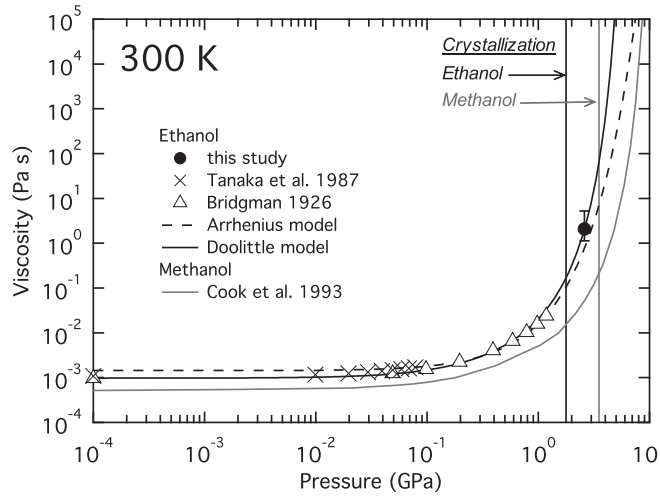

FIG. 5. Dependence of viscosity on pressure for ethanol (black) and methanol (grey) at room temperature. The present estimate for ethanol at 2.6 GPa is the black circle, based on the corrected Arrhenius dependence at this pressure [Fig. 2(b)] extrapolated to room temperature. Prior measurements are crosses [21] and triangles [13]. Curves are the initial Arrhenius model for ethanol [dashed, using Eq. (1) with parameters fitted to low pressure data], a Doolittle fit [Eq. (6)] to all the ethanol data (solid), and the previously measured dependence for methanol (solid grey) [11]. Equilibrium crystallization pressures are vertical lines [17], beyond which viscosity is found to rise sharply in a similar manner for both ethanol and methanol.

viscosity at pressure. A global Arrhenius fit to viscosity data on ethanol, including the values inferred at high pressure and temperature from analysis of the present data, is shown in Fig. 4. Final best fit parameters are $B = 4.89(34) \times 10^{-6}$ Pa s, $E_{act0} = 0.139(1)$ eV, and $V_{act} = 0.0758(4)$ eV/GPa.

The adjusted Arrhenius model implies an effective room temperature viscosity at 2.6 GPa of $\eta = 2.1(^{+3.2}/_{-1.0})$ Pa s, yielding a sharper increase in viscosity with pressure than initially estimated (Fig. 5). The form of the viscosity increase in ethanol thus determined is strikingly similar to that observed in methanol under pressure [11]. Compared to methanol, where the liquid may be compressed beyond its normal freezing pressure, viscosity measurements near room temperature on ethanol are limited by relatively easy crystallization [11,17]. The approach outlined here thus enables a first comparison of viscosities in the ultrahigh pressure regime for these alcohols, beyond room-temperature freezing pressures, and approaching glass transitions.

The rapid increase in viscosity begins at lower pressure in ethanol compared to methanol, consistent with its significantly lower equilibrium crystallization point under pressure (1.78 GPa compared to 3.51 GPa) [17]. As for methanol, ethanol data are well fit by a Doolittle model,

$$\eta = M \exp\left(\frac{NV_{inf}}{V - V_{inf}}\right), \tag{6}$$

which describes the sharp increase in viscosity as liquid is superpressed beyond its freezing point [11]; V is the volume at pressure P (Ref. [24]), V_{inf} is the volume at infinite viscosity, and M and N are constants. The glass transition pressure, inferred as where the viscosity reaches a value of 10^{12} Pa s (Refs. [26,27]), similarly scales with normal solidification pressure as 6.3 GPa for ethanol and 11.4 GPa for methanol [27], or 3.4(1) times the equilibrium crystallization pressures. This resembles the correlation between the conditions of crystallization and glassification observed at room pressure [26,28]. The viscosity at the equilibrium solidification pressures is 0.19(2) Pa s, again showing the similarity in properties of these alcohols, irrespective of whether they more readily crystallize or form glass to higher pressures.

The Reynolds number Re of the observed flows, or

$$\mathrm{Re} = \frac{U\rho D}{\eta}, \tag{7}$$

is of order 10^{-6}–10^{-4} (Table I) indicative of a highly laminar flow regime, consistent with the numerical modeling and assumptions. The Rayleigh number Ra of the system, used to assess convection activity, is

$$\mathrm{Ra} = \frac{\rho^2 g \alpha C_P \Delta T D^3}{\eta \kappa}, \tag{8}$$

where C_P is the heat capacity at constant pressure and κ is the thermal conductivity. Ra is of order 10^{-2}–10^{-1} for our system (Table I, Fig. 2), below values typically associated with thermal convection. Convection in the present case is possible due to the irregular geometry of the laser-heated DAC [8,23].

The arrangement of the sample in this experiment, where gravity is oriented transverse to the sample cavity layer, should optimize the vigor of flow and hence its visibility. It also provides predominantly transverse flow, so the measured (i.e., transverse) speed of fluid motion equals the local convective flow speed. Thus, the presently used experimental configuration is superior to that previously described [8] for the purposes of observing convective motions in

the DAC and using these to assess the sample's transport properties.

IV. CONCLUSIONS

Our results demonstrate that it is possible to create and characterize natural convection on the extremely small length scales of high pressure samples (with typical sample thickness of order microns), confirming qualitative assessments of prior experiments [4–7]. The existence of convective instability and detectable flow is attributed to the especially large temperature gradients and absence of simple symmetry in the liquid region [8,23], which compensate for the small length scale. Moreover, we find that flow observations can be used to determine fluid transport properties at extremes. This is achieved using scaling laws and through detailed analysis of the microscale flow with numerical modeling, including optimizing models to fit the measurements of convective speed inside the molten sample at pressure.

Consistent with previous measurements in ethanol to 1.2 GPa and mirroring the behavior of methanol at higher pressures, we find a sharp rise in the viscosity of ethanol above the normal crystallization pressure at room temperature in the region of 2–3 GPa, associated with the approach to glass transition. By enabling viscometry at previously unexamined pressures where ethanol crystallizes at room temperature, this approach extends measurements of viscosity beyond the original data of Bridgman [13].

With the accessible pressure and temperature range of the laser-heated DAC far exceeding that of traditional methods for measuring viscosity at high pressures, detection and analysis of the intrinsic convection in melted samples is a plausible method to extend viscosity measurement to unprecedented extreme conditions. Such observations can further address many longstanding questions about high-pressure melting, such as regarding the relationships between melt temperature, liquid structure, and flow behavior. The extremely low Rayleigh number of such flows also suggests a unique fluid-dynamical regime of fundamental physical interest.

ACKNOWLEDGMENTS

This work was supported by an EPSRC First Grant (Grant No. EP/P024513/1), a Carnegie Trust Research Incentive Grant (Grant No. 70249), the British Council Researcher Links Programme, and a Leverhulme Trust Grant (Grant No. RPG-2017-035). Thanks to Jochen Arlt and Andrew Garrie for experimental assistance.

[1] H. Terasaki and R. A. Fischer, *Deep Earth: Physics and Chemistry of the Lower Mantle and Core* (John Wiley & Sons, Inc., Hoboken, New Jersey, 2016), Vol. 217.
[2] Y. Wang, T. Sakamaki, L. B. Skinner, Z. Jing, T. Yu, Y. Kono, C. Park, G. Shen, M. L. Rivers, and S. R. Sutton, Nat. Commun. **5**, 3241 (2014).
[3] M. Ross, D. Errandonea, and R. Boehler, Phys. Rev. B **76**, 184118 (2007).
[4] G. Shen, P. Lazor, and S. K. Saxena, Phys. Chem. Miner. **20**, 91 (1993).
[5] R. Boehler, Nature **363**, 534 (1993).
[6] R. Jeanloz and A. Kavner, Philos. Trans. R. Soc. London A **354**, 1279 (1996); P. Lazor and S. K. Saxena, *ibid.* **354**, 1307 (1996).
[7] D. Errandonea, J. Phys. Chem. Solids **67**, 2017 (2006).
[8] N. Gomez-Perez, J. F. Rodriguez, and R. S. McWilliams, J. Appl. Phys. **121**, 145904 (2017).
[9] P. M. Celliers, M. Millot, S. Brygoo, R. S. McWilliams, D. E. Fratanduono, J. R. Rygg, A. F. Goncharov, P. Loubeyre, J. H. Eggert, J. L. Peterson, N. B. Meezan, S. Le Pape, G. W. Collins, R. Jeanloz, and R. J. Hemley, Science **361**, 677 (2018).
[10] K.-I. Funakoshi, High Press. Res. **30**, 60 (2010).
[11] R. L. Cook, C. A. Herbst, and H. E. King, Jr., J. Phys. Chem. **97**, 2355 (1993).
[12] E. H. Abramson, J. Phys. Chem. B **118**, 11792 (2014).
[13] P. W. Bridgman, Proc. Am. Acad. Arts Sci. **61**, 57 (1926).
[14] E. H. Abramson, Phys. Rev. E **76**, 051203 (2007).
[15] A. F. Goncharov, J. A. Montoya, N. Subramanian, V. V. Struzhkin, A. Kolesnikov, M. Somayazulu, and R. J. Hemley, J. Synchrotron Radiat. **16**, 769 (2009).
[16] H. K. Mao, J. Xu, and P. M. Bell, J. Geophys. Res. **91**, 4673 (1986).
[17] J. F. Mammone, S. K. Sharma, and M. Nicol, J. Phys. Chem. **84**, 3130 (1980).
[18] M. V. Kondrin, A. A. Pronin, and V. V. Brazhkin, J. Chem. Phys. **141**, 194504 (2014).
[19] J.-Y. Tinevez, N. Perry, J. Schindelin, G. M. Hoopes, G. D. Reynolds, E. Laplantine, S. Y. Bednarek, S. L. Shorte, and K. W. Eliceiri, Methods **115**, 80 (2017).
[20] Z. Konôpková, R. S. McWilliams, N. Gómez-Pérez, and A. F. Goncharov, Nature **534**, 99 (2016).
[21] Y. Tanaka, Y. Matsuda, H. Fujiwara, H. Kubota, and T. Makita, Int. J. Thermophys. **8**, 147 (1987).
[22] R. L. Cook, H. E. King, C. A. Herbst, and D. R. Herschbach, J. Chem. Phys. **100**, 5178 (1994).
[23] M. Manga and R. Jeanloz, in *Properties of Earth and Planetary Materials at High Pressure and Temperature*, Geophys. Monogr. Set., edited by M. Manghnani (AGU, Washington, D.C., 1998), Vol. 101, pp. 17–25.
[24] J. M. Brown, L. J. Slutsky, K. A. Nelson, and L.-T. Cheng, Science **241**, 65 (1988).
[25] W. Haynes, *CRC Handbook of Chemistry and Physics,* 100th ed. (National Institute of Standards and Technology, Boulder, CO, 2019).
[26] D. Turnbull, Contemp. Phys. **10**, 473 (1969).
[27] C. A. Herbst, R. L. Cook, and H. E. King, Special issue on relaxations in complex systems, J. Non-Cryst. Solids **172–174**, 265 (1994).
[28] R. F. Fedors, J. Polym. Sci.: Polym. Lett. Ed. **17**, 719 (1979).